Geochimica et Cosmochimica Acta Vol. 54, pp. 1817–1833

0016-7037/90/$3.00 + .00

The significance of fractional crystallization in the petrogenesis of Apollo 17 Type A and B high-Ti basalts

CLIVE R. NEAL,[1] LAWRENCE A. TAYLOR,[1] SCOTT S. HUGHES,[2,*] and ROMAN A. SCHMITT[2]
[1]Department of Geological Sciences, University of Tennessee, Knoxville, TN 37996, USA
[2]Radiation Center, Oregon State University, Corvallis, OR 97331, USA

(*Received August* 23, 1989; *accepted in revised form March* 22, 1990)

Abstract—Whole-rock and mineral analyses of 26 "new" Type A and B Apollo 17 basalts are reported. The petrography and mineral chemistry of these basalts are similar to previously reported Apollo 17 basalts. However, these "new" whole-rock data extend the compositional ranges of previously reported Type A and B basalts and require the division of the Type B basalts into Type B1 and B2 varieties. These *three* types display similar trends when both major and trace elements are plotted against a fractionation index of Cr/La ratio. Major element compositions of basalts from all three types fall on olivine + Ti oxide control lines. The compositional ranges of all three groups can be effectively generated by 40–50% fractional crystallization of observed phenocryst phases. The compositions of three Type A basalts are only generated after 80% fractional crystallization. Previous models of different degrees of partial melting and KREEP assimilation were developed in order to explain the range in La/Sm ratio of the Type B basalts. With the recognition of two types of "B" basalts, these models are no longer valid. This study demonstrates that Apollo 17 Type A, B1, and B2 basalts have a relatively simple petrogenesis, with the only post-magma-generation process being fractional crystallization.

INTRODUCTION

THE PRESENCE ON THE MOON of basalts containing more than 10 wt% TiO_2 highlights the differences in lunar and terrestrial mantle compositions. These lunar basalts are derived from the part of the mafic cumulate portion which forms the lower crust/upper mantle of the Moon as a result of Lunar Magma Ocean (LMO) crystallization. As partial melts from this region, these samples provide us with a vast array of chemical data which give indications as to the nature of the source region(s) and possible contamination by crustal materials.

Three types of high-Ti basalt (A, B, and C) were recognized in the Apollo 17 samples by RHODES et al. (1976) on the basis of whole-rock chemistry. Type A basalts contain 50–60% higher abundances of incompatible trace elements than do the Type B basalts (WARNER et al., 1979), although Type A and B basalts possess similar major-element compositions. Type B basalts possess a range in the La/Sm ratio (not observed in Type A and C) that cannot be explained by near-surface fractional crystallization of a single parental magma (WARNER et al., 1979). The Type C variety is found only at Station 4 (Shorty Crater), and only five examples are known (NEAL et al., 1989a; RHODES et al., 1976; WARNER et al., 1979). Type C basalts contain higher MgO and Cr_2O_3 contents than the Type A and B basalts. Furthermore, the compositional differences *between* the three groups cannot be explained by near-surface crystallization, requiring that these basalt types were derived from distinct source regions (SHIH et al., 1975; RHODES et al., 1976; WARNER et al., 1979).

Previous work has emphasized the processes of partial melting and near-surface fractional crystallization in the petrogenesis of these basalts (LONGHI et al., 1974; SHIH et al., 1975; RHODES et al., 1976; WARNER et al., 1979). NEAL et al. (1989a) suggested that Type A and B basalts could have been derived from a common source, but experienced different post-magma-generation processes; Type B basalts underwent assimilation of Apollo 17 KREEP while fractionating observed phenocryst phases (AFC), whereas Type A basalts only experienced fractional crystallization. Progressive KREEP assimilation was required in order to generate the range in La/Sm ratios of the Type B basalts observed by WARNER et al. (1979).

The aims of this paper are (1) to present petrographic and mineralogic data for 26, and whole-rock data for 25, previously unanalyzed Apollo 17 high-Ti basalts, which turned out to be all of Type A and B; and (2) to integrate these data with that already available for Type A and B basalts in order to constrain their petrogenesis. This study tests previous petrogenetic models, including our own, and presents a working hypothesis of magmatic evolution experienced by the Apollo 17 high-Ti basalts.

PETROGRAPHY

Previous chemical and petrographic investigations had each suggested the presence of three basalt types (PAPIKE et al., 1974; BROWN et al., 1975; DYMEK et al., 1975; WARNER et al., 1975, 1979; RHODES et al., 1976; NEAL et al., 1989b). However, these divisions do not correspond with each other. Indeed, all three of these petrographic types are present in each chemical group. The petrographic varieties are **Type 1A** = *olivine porphyritic ilmenite basalt*, usually quenched and olivine-rich; **Type 1B** = *plagioclase-poikilitic ilmenite basalt*, coarse-grained (slower cooling) and olivine-poor; **Type II** = *Apollo 11, low-K-type basalt* (olivine-free). In our suite of 26 "new" Apollo 17 basalts, we have 8 Type 1A basalts (fine-

* *Present address:* Montana Bureau of Mines & Geology, Montana College of Mineral Science and Technology, Butte, MT 59701, USA.

grained olivine-porphyritic), 17 Type 1B basalts (plagioclase-poikilitic), and 1 Type II (olivine-free, Apollo 11 low-K-type). The general petrographic features and the modal mineralogy of these basalts are presented in Table 1.

The Type 1A olivine-porphyritic ilmenite basalts are all fine-grained (typically <1 mm) with a general subvariolitic texture (Fig. 1a). The one exception is 71157, which is vitrophyric (Fig. 1b). All Type 1A basalts contain both olivine and ilmenite phenocrysts (Fig. 1a,b). Armalcolite, where present, forms cores to ilmenite (71157: Fig. 1c), is partially rimmed by ilmenite (74285), or is present as discrete grains ~ 0.2 mm (71097). Chromite-ulvöspinel is present either as discrete grains (0.1–0.3 mm) or as inclusions in olivine (<0.1 mm). All Type 1A basalts contain "sawtooth" ilmenites (Fig. 1a–c), indicative of rapid crystallization (e.g., PAPIKE et al., 1974). Pink pyroxene prisms (~0.4 mm) and plagioclase laths (~0.3 mm) are usually interstitial, sometimes combining to form small "bowtie" textures. Plagioclase is present in the vitrophyre 71157, but the laths are too thin (<3 μm) to probe. Phenocryst phases present in this sample are olivine, armalcolite, ilmenite, and minor spinel.

All plagioclase-poikilitic (Type 1B) basalts are coarse-grained (>2 mm: Fig. 1d), except for 74287, which is medium-grained (grain size ~ 1 mm), but olivine-poor. In all cases, ilmenite exsolved both ulvöspinel and rutile which are present as thin (<0.05 mm wide) lamellae within the ilmenite. Armalcolite and discrete chromite-ulvöspinel (0.2–0.5 mm and 0.1–0.2 mm), where present, are inclusions in olivine, pyroxene, and/or plagioclase (Fig. 1e). Some armalcolites possess a discontinuous ilmenite overgrowth. Most olivine (up to 0.4 mm) is present (except in 70147) as either discrete inclusions in plagioclase or as the cores of pyroxenes. It is likely that olivine in 70147 has been totally resorbed by the magma and has been replaced by pyroxene. The petrographic relationships of the minerals indicate that these basalts have fractionated clinopyroxene (i.e., titan-augite) after olivine. Plagioclase-poikilitic basalts commonly contain interstitial SiO_2 (tridymite ~ 0.1 mm) and also native Fe and troilite (Fig. 1c).

One Type II, Apollo 11, low-K-type, high-Ti basalt is represented in this study of Apollo 17 high-Ti basalts. 71095 is a medium-grained (up to 1.5 mm) sub-ophitic basalt (Fig. 1f). Subhedral ilmenite (0.1–3.1 mm) is the only opaque phase present; it exhibits smooth grain boundaries and contains ulvöspinel and rutile exsolution lamellae (<0.05 mm). No olivine is present. Interstitial, late-stage SiO_2 (up to 0.6 mm) is present, as is interstitial native Fe and troilite (both ~ 0.1 mm).

Modes for each of the basalts were determined by point counting (~1500 points per thin section) and results are presented in Table 1. Generally, the olivine porphyritic (Type 1A) basalts contain more olivine than the plagioclase-poikilitic Type 1B basalts. Ilmenite, armalcolite, and chromite-ulvöspinel tend to be present in similar proportions in both Type 1A and 1B basalts, but not in the Apollo 11 low-K-type (Type II) basalt. As expected, plagioclase is more abundant in the Type 1B plagioclase-poikilitic varieties.

MINERAL CHEMISTRY

Mineral compositions of the 26 new Apollo 17 basalts were determined on a Cameca SX-50 electron microprobe at the

TABLE 1: Modal Analyses for Apollo 17 Titaniferous Basalts. SP = Spinel (Chromite-Ulvöspinel); ME = Native Fe + Troilite; @ = laths too thin to probe.

SAMPLE	TEXTURE	TYPE	OL	PX	PLAG	ILM	ARMAL	SP	ME	SiO_2	GLASS
71048,3	FG(OP)	1A	7.6	39.5	20.4	28.4	—	0.4	2.8	—	0.9
71087,4	FG(OP)	1A	0.2	48.1	24.4	21.2	—	2.0	3.1	1.0	—
71088,4	FG(OP)	1A	8.2	36.8	28.0	21.7	—	2.1	2.3	0.9	—
71096,4	FG(OP)	1A	7.1	44.0	24.6	21.3	1.5	—	1.3	0.2	—
71097,3	FG(OP)	1A	6.8	43.9	23.1	23.4	0.5	0.5	1.1	0.7	—
71157,4	V(OP)	1A	2.7	27.9	7.2@	13.7	7.5	2.5	1.1	—	37.4
74286,3	FG(OP)	1A	2.1	43.5	25.9	22.7	—	2.5	3.1	0.2	—
79265,4	FG(OP)	1A	1.0	49.7	28.1	17.2	—	0.4	2.1	1.4	0.1
70138,3	PP	1B	3.0	49.7	22.2	21.1	3.0	—	1.0	—	—
70139,3	PP	1B	2.5	35.8	41.6	15.8	—	—	2.4	1.9	—
70145,3	PP	1B	1.9	40.5	32.5	20.6	2.4	0.8	1.3	—	—
70146,4	PP	1B	2.1	41.5	33.3	19.6	0.5	—	3.0	—	—
70147,4	PP	1B	—	48.2	29.4	16.7	0.5	0.5	4.5	0.2	—
70148,3	PP	1B	1.0	40.9	30.5	17.9	0.9	0.5	4.0	4.3	—
70155,3	PP	1B	1.9	47.0	29.6	16.3	1.5	0.6	2.8	0.3	—
70156,4	PP	1B	2.3	65.2	7.7	19.7	2.9	—	2.2	—	—
70157,4	PP	1B	0.4	55.2	24.7	16.0	1.0	—	2.7	—	—
70165,3	PP	1B	0.9	40.2	33.8	13.7	—	—	6.3	2.3	2.8
71047,3	PP	1B	1.1	48.2	26.3	21.1	0.2	0.4	1.8	0.9	—
71049,3	PP	1B	0.2	41.6	31.0	22.5	—	—	2.7	2.0	—
71089,4	PP	1B	0.3	45.1	23.3	24.9	—	—	3.9	2.5	—
75065,4	PP	1B	1.0	49.9	23.4	20.4	0.9	1.1	1.5	1.8	—
75086,3	PP	1B	1.3	51.3	26.3	18.2	1.3	—	1.6	—	—
75087,3	PP	1B	0.4	48.9	19.8	21.0	—	—	6.6	3.3	—
76037,4	PP	1B	0.5	45.6	33.1	17.5	—	0.6	1.4	1.0	0.3
71095,4	SO	II	—	44.0	37.6	11.7	—	—	3.4	3.3	—

FG(OP) = Fine-Grained, Olivine Porphyritic; V(OP) = Vitrophyric, Olivine Porphyritic; SO = Sub-Ophitic; PP = Plagioclase-Poikilitic.

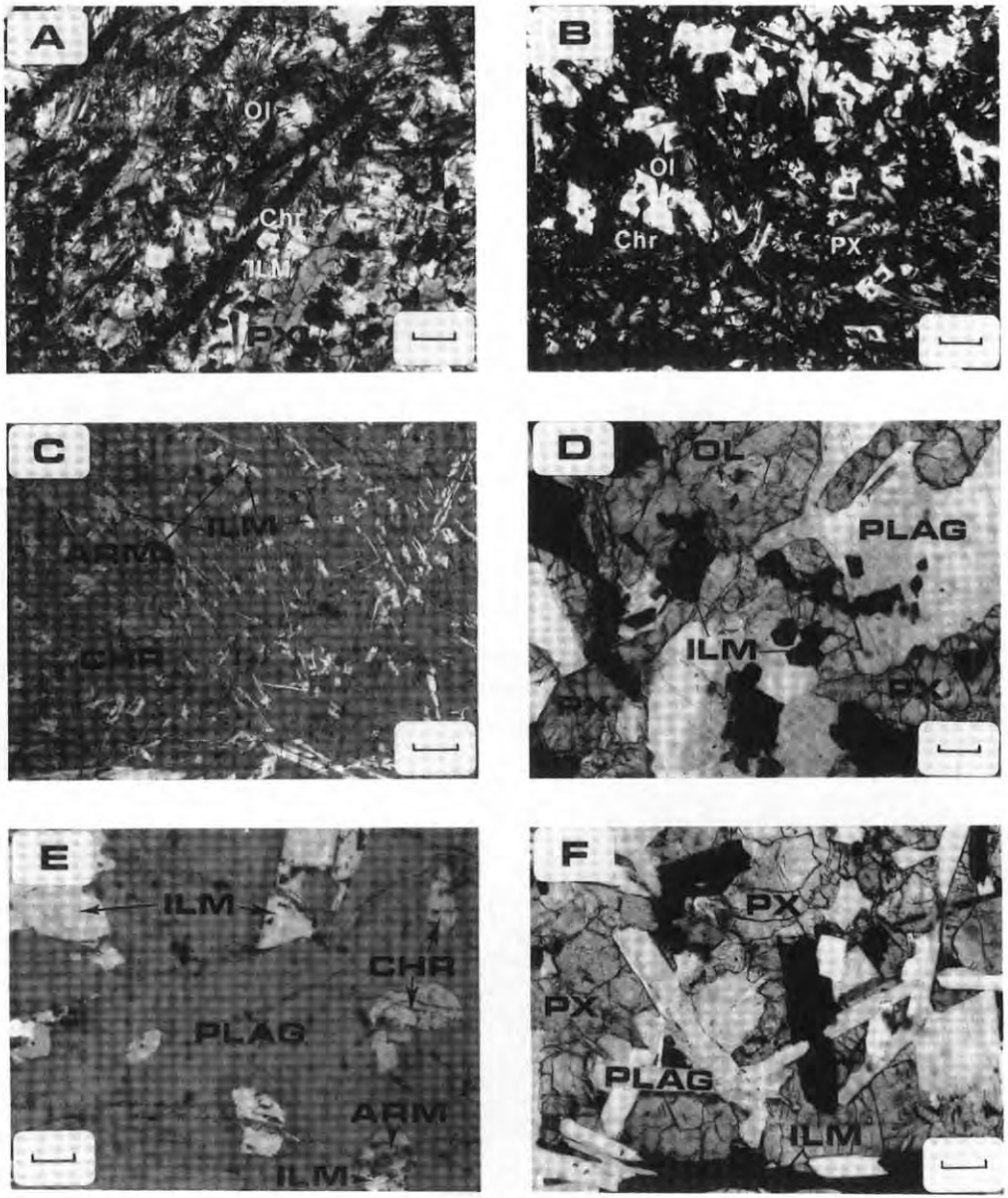

FIG. 1. Representative photomicrographs highlighting the salient features of the Apollo 17 high-Ti basalts analyzed in this study. CHR = Chromite-Ulvöspinel; OL = Olivine; ILM = Ilmenite: PX = Pyroxene; ARM = Armalcolite. a) Photomicrograph of Type 1A basalt 71048 from thin section ,3. Note olivine microphenocrysts and ilmenite phenocrysts and general subvariolitic texture, typical of petrographic Type 1A or Apollo olivine-porphyritic ilmenite basalts from Apollo 17. Ilmenites commonly exhibit "sawtooth" margins, indicative of relatively rapid cooling. Scale bar represents 0.2 mm. b) Photomicrograph of Type 1A basalt 71157 from thin section ,4. This basalt contains more glass than the typical Type 1A varieties. Olivine phenocrysts commonly contain euhedral inclusions of chromite. Scale bar represents 0.2 mm. c) The same view of 71157, but seen in reflected light. Most of the ilmenite phenocrysts contain armalcolite cores. Scale bar represents 0.2 mm. d) Photomicrograph of Type 1B basalt 70146 from thin section ,4. This basalt is typical of the petrographic Type 1B or plagioclase poikilitic Apollo 17 basalts. Scale bar represents 0.2 mm. e) Photomicrograph of basalt Type 1B 70156 from thin section ,4 seen in reflected light. Here, discrete ilmenites and chromite-ulvöspinels are enclosed in plagioclase. Armalcolite is also present as inclusions in plagioclase, and may possess a discontinuous rim of ilmenite. Scale bar represents 0.05 mm. f) Photomicrograph of Type II basalt 71095 from thin section ,4 depicting the only petrographic Type II (Apollo 11-low-K-type) Apollo 17 basalt found in this study. Note the general sub-ophitic texture. Scale bar represents 0.2 mm.

University of Tennessee. Accelerating voltage was 15 kV with a filament current of 100 μA. Beam current used for all phases was 30 nA, except for feldspars and glasses when 20 nA was employed (beam current was measured by a Faraday cup); counting times were 20 sec for each element. All data were corrected using ZAF procedures. The variation in mineral compositions are given in Table 2.

Pyroxene

Generally, both Type 1A and 1B pyroxenes exhibit similar compositional trends, with both Ca- and Mg-rich varieties trending towards Fe enrichment (Fig. 2a,b; Table 2). However, the Apollo 11 low-K-type basalt contains only titanaugites trending towards Fe enrichment (Fig. 2c). Pyroxenes from all petrographic types contain Al/Ti ratios clustering around 2. As Fe increases, total Ti and Al decrease, but maintain a Al/Ti of 2. Cr_2O_3 is in some cases greater than 1 wt%, but decreases with Fe enrichment. Core-to-rim zonation varies from Ca-to-Mg-to-Fe or Mg-to-Fe, and Ca-to-Fe as in the case of the Apollo 11 low-K-type basalts. These observations are similar to those described by PAPIKE et al. (1974), BROWN et al. (1975), DYMEK et al. (1975), and WARNER et al. (1975) for pyroxenes from Apollo 17 high-Ti basalts. Titanaugite was the first pyroxene to crystallize. Pigeonite followed with the resorption of early formed olivine (PAPIKE et al., 1974). The vitrophyric basalt 71157 contains pyroxenes of a very restricted composition (Fig. 2d). These pyroxenes contain Al/Ti ratios > 2 (NEAL et al., 1989b), indicating rapid cooling with pyroxene crystallizing before plagioclase.

Olivine

By definition, olivine is only present in Type 1A and 1B basalts (Table 2). In the Type 1A (olivine porphyritic) basalts, zonation of olivines is marked in large (>0.7 mm) olivine phenocrysts from cores of Fo_{78-69} to rims of Fo_{65-51} (e.g., 71087). Smaller olivines exhibit less marked zonations but are generally more Fa rich than the larger varieties. In Type 1B (plagioclase-poikilitic), olivines exhibit little core-to-rim zonation, but variation between different olivine grains is noted.

Plagioclase

Plagioclase exhibits similar compositional zonations in each group from An-rich (An_{87-92}) to Ab-rich rims (Ab_{15-26}) (Table 2). This suggests late-stage plagioclase crystallization, especially in the Type 1B plagioclase-poikilitic types, as indicated by the crystallization experiments of USSELMAN et al. (1975).

Ilmenite

Ilmenites from all textural groups contain Cr_2O_3 up to 0.9 wt% but exhibit little core-to-rim zonation, even the mantles on armalcolite (e.g., 71157). The variations noted in Table 2 are among individual grains. No distinction between the textural groups can be made using the MG# [100*(Mg/(Mg + Fe))] of ilmenite.

Armalcolite

Armalcolite contains up to 1.2 wt% Cr_2O_3. Core-to-rim zonation is slight, but discernable towards more Fe-rich compositions, especially where mantled by ilmenite (e.g., 71157). Discrete armalcolites are usually homogeneous.

TABLE 2: Textural Type and Mineral Compositions of Apollo 17 Titaniferous Basalts.

SAMPLE	TYPE	OLIVINE	PLAGIOCLASE		PYROXENE		CHROMITE	ILMENITE	ARMAL
PM		Fo	An	Ab	Wo	En	Cr#	Mg#	Mg#
71048,3	1A	63-66	78-86	12-18	16-46	15-48	70-78	6-9	7-12	---
71087,4	1A	58-71	81-87	13-18	11-46	27-54	65-76	4-18	2-12	---
71088,4	1A	43-71	80-88	11-17	7-46	26-64	72-77	7-8	7-18	---
71096,4	1A	57-70	78-94	5-19	8-45	20-61	---	---	2-18	36-41
71097,3	1A	60-72	78-88	11-20	9-49	33-56	70-73	7-9	2-15	40-42
71157,4	1A	63-75	---	---	45-49	30-35	67-69	15-17	8-13	37-50
74286,3	1A	63-71	78-90	10-19	6-48	24-58	69-77	3-20	5-24	---
79265,4	1A	51-68	80-88	12-19	8-41	21-62	74-75	3-11	2-8	---
70138,3	1B	48-69	84-89	11-16	7-40	27-67	---	---	5-23	43-45
70139,3	1B	55-69	71-88	11-26	8-39	11-65	---	---	10-22	---
70145,3	1B	60-73	85-92	8-15	7-39	45-67	68-83	13-26	10-26	42-46
70146,4	1B	66-68	72-88	11-24	7-39	21-66	---	---	3-19	43-45
70147,4	1B	—	76-90	10-22	7-42	43-65	64-69	20-24	6-13	39-46
70148,3	1B	63-66	76-89	11-21	8-41	16-65	69-70	24-25	4-11	44-46
70155,3	1B	58-67	72-90	9-22	7-42	29-67	77-78	11-12	7-14	43-46
70156,4	1B	68-70	77-81	18-22	11-42	27-51	---	---	5-14	27-46
70157,4	1B	62-70	84-89	10-15	7-41	43-66	---	---	8-29	27-46
70165,3	1B	49-64	78-92	8-19	5-43	21-64	---	---	3-19	---
71047,3	1B	49-73	74-89	11-23	8-43	26-64	66-68	24-25	7-29	43-45
71049,3	1B	57-67	79-89	11-19	7-43	30-66	---	---	6-11	---
71089,4	1B	55-67	79-91	9-19	8-43	27-61	---	---	9-21	---
75065,4	1B	45-70	71-89	11-24	7-43	31-61	49-70	20-34	6-24	42-44
75086,3	1B	58-67	79-88	12-20	7-43	37-66	---	---	6-19	43-46
75087,3	1B	37-65	75-90	10-23	7-40	31-61	---	---	7-20	---
76037,4	1B	50-65	78-88	11-20	8-40	25-63	71-73	14-16	6-17	---
71095,4	II	---	72-88	11-22	16-40	6-49	---	---	1-10	---

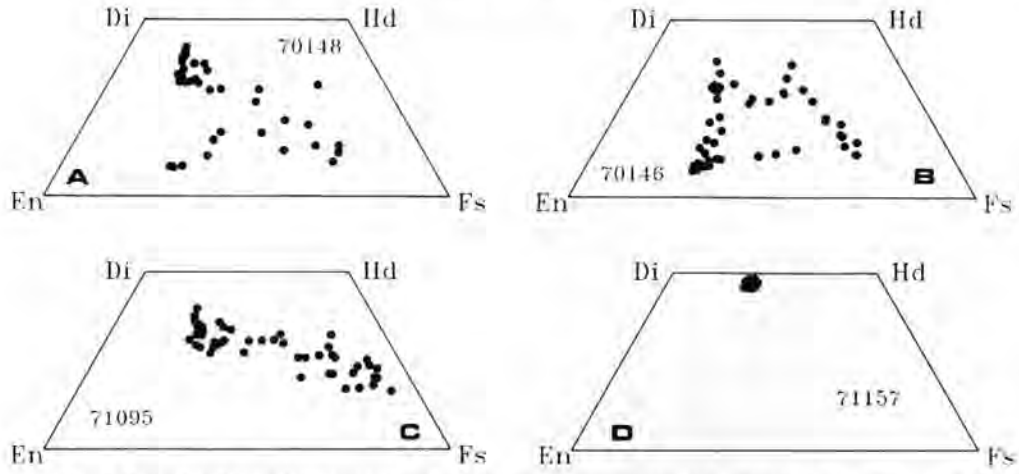

FIG. 2. Examples of the various compositional trends observed in pyroxenes from the Apollo 17 high-Ti basalts.

Spinel Phases

Most spinels are inclusions in olivine or exsolution products from ilmenite, but discrete grains are rare. When armored by olivine, spinels are of the chromite-ulvöspinel series and are homogeneous. However, where discrete or included in pyroxene which has replaced olivine (as witnessed by petrography), the spinels are zoned towards more ulvöspinel-rich and Cr- and Mg-poor compositions. Al_2O_3 is approximately constant from core-to-rim. This zonation indicates an interaction of early formed chromite with the evolving magma.

Metal

All but two of the Apollo 17 basalts studied here contain metals possessing less than 2 wt% Co and less than 1 wt% Ni (NEAL et al., 1989b), although some metals can contain approximately 12–15 wt% Ni and 7–8 wt% Co. The relatively high Co/Ni ratio of these metals, coupled with generally low Ni abundances, indicates the probable pristinity of these basalts. Even those with high Ni contents possess high Co/Ni ratios.

Glass

Interstitial glass is found in some, but not all, of the basalts. It is especially abundant in the Type 1A basalts (olivine porphyritic). Generally, it is high in silica, Al_2O_3, and K_2O (70–88 wt%, 7–15 wt%, 2–9 wt%, respectively), with low FeO, TiO_2, and Na_2O (<1 wt%, 0.9–1.4 wt%, and <1 wt%, respectively) and moderate CaO (0.4–6 wt%). This glass is not the high-silica endmember of immiscibility, as discussed by NEAL and TAYLOR (1989); no corresponding low-silica glass is present, no immiscibility textures are present, and the CaO content of the glass is generally too high. Rather, with much Fe-Ti-oxide crystallization, the residual magma underwent a silica enrichment with Fe depletion, thus missing the immiscibility gap (HESS et al., 1975; RYERSON and HESS, 1980). The opaque glass in the vitrophyric basalt 71157 represents the residual magma after minor crystallization. This glass contains ~54 wt% SiO_2, ~16 wt% Al_2O_3, ~11 wt% FeO, ~1.2 wt% Na_2O, <1 wt% K_2O, ~2 wt% TiO_2, and ~10 wt% CaO.

WHOLE-ROCK CHEMISTRY

The whole-rock compositions of the 25 "new" Apollo 17 high-Ti basalts were determined by INAA at Oregon State University. The whole-rock analysis for the 26th basalt has not been carried out as the sample was not available at the time of this INAA run. The general analytical procedures and errors involved can be found in SIMON et al. (1989).

Previous workers (e.g., RHODES et al., 1976; WARNER et al., 1979) noted that data from coarse-grained plagioclase-poikilitic basalts appeared to plot as clouds about the arrays defined by fine-grained varieties. This scatter was attributed to unrepresentative sampling of these coarse-grained basalts. As many of our "new" basalts are coarse-grained, we have significantly reduced these sampling errors by either homogenizing by crushing of a large chip (22 samples—see Table 3) or crushing and taking a 50% split of the homogenized fines (70139,4, 70145,4, and 70146,0). Where possible, we have analyzed a relatively large sample of each basalt (up to 0.8 g). Although the sampling errors have been reduced, it is still possible that some scatter may still occur. However, we assume that our analyses of these coarse-grained basalts are representative of the whole-rock composition and not a function of sampling errors. Furthermore, we will demonstrate that our data are consistent with previously determined whole-rock compositions for fine-grained Apollo 17 high-Ti basalts.

Results

Whole-rock chemistry of the Apollo 17 high-Ti basalts suggested three distinct chemical types—A, B, C in the classifications of WARNER et al. (1975, 1979) and RHODES et al. (1976). All the petrographic groups outlined above are found

TABLE 3: Whole-rock analyses (by INA) of 25 "new" Type A and B Apollo 17 High-Ti basalts. Major element abundances are in wt% oxides and trace elements are reported in ppm.

SAMPLE	70138,4	70145,4	70146,0	70147,0	70165,4	71048,4	71049,4	71087,5
TYPE	A	A	A	A	A	A	A	A
Wt (g)	0.7522	0.5725	0.4082	0.6364	0.5309	0.3338	0.5172	0.5596
TiO_2	12.5	13.5	13.1	13.0	12.7	12.9	12.5	12.9
Al_2O_3	8.5	7.8	7.6	8.4	8.4	8.7	8.2	8.1
FeO	17.9	19.0	19.6	17.9	17.9	18.3	17.8	18.8
MnO	0.237	0.256	0.255	0.231	0.247	0.253	0.249	0.250
MgO	8.2	8.5	8.8	8.8	8.7	8.0	8.3	7.9
CaO	9.5	9.2	9.7	9.2	10.2	10.2	9.8	10.2
Na_2O	0.39	0.36	0.36	0.39	0.38	0.39	0.39	0.39
K_2O	0.05	0.08	0.05	0.06	0.06	0.07	0.07	0.08
MG#	44.9	44.4	44.4	46.7	46.4	43.8	45.4	42.8
Sc	77	82	85	77	82	86	81	81
V	134	130	126	131	114	105	125	104
Cr	3430	3440	3450	3530	3140	2990	3080	2960
Co	19.8	18.4	21.6	22.8	18.0	19.5	19.1	18.7
Ni	4	19	5	6	23	56	27	28
Sr	170	240	---	140	160	140	300	190
Cs	0.11	0.11	0.07	0.04	0.13	0.13	0.07	0.10
Ba	65	103	104	76	111	129	104	89
La	5.1	6.2	6.3	4.8	5.7	6.6	6.2	6.5
Ce	24	32	29	22	23	30	26	23
Nd	20	25	26	18	21	29	26	25
Sm	7.6	9.5	9.5	7.1	8.6	9.9	9.4	9.5
Eu	1.9	2.1	2.0	1.7	1.9	2.1	2.0	2.0
Tb	2.1	2.4	2.7	2.1	2.6	2.6	2.7	2.7
Dy	15.8	18.5	17.4	13.2	15.9	18.7	17.8	18.6
Yb	7.5	9.2	9.4	7.2	8.4	9.5	8.8	9.4
Lu	1.12	1.35	1.33	1.07	1.22	1.39	1.31	1.33
Zr	230	180	250	210	130	170	---	340
Hf	7.3	8.7	8.8	6.9	7.9	9.4	8.6	8.7
Ta	1.6	1.7	1.8	1.4	1.5	1.8	1.7	1.7
Th	0.1	0.3	0.1	0.2	0.1	0.3	0.4	0.1
U	0.2	0.5	0.1	0.1	0.1	0.1	0.3	---
La/Sm	0.668	0.660	0.656	0.670	0.671	0.661	0.661	0.680
Cr/La	679	551	552	743	547	455	494	457

TABLE 3: Cont.

SAMPLE	71088,5	71095,0	71096,5	74286,4	75065,0	75086,4	75087,4	79265,5
TYPE	A	A	A	A	A	A	A	A
Wt (g)	0.3312	0.7839	0.5992	0.5660	0.9090	0.5067	0.5458	0.3852
TiO_2	12.5	7.7	13.0	12.2	12.7	12.5	13.4	11.8
Al_2O_3	8.6	9.8	7.9	8.7	8.3	8.0	7.4	8.8
FeO	18.5	18.9	19.9	18.9	18.8	19.5	19.2	19.2
MnO	0.260	0.257	0.258	0.254	0.247	0.245	0.254	0.253
MgO	8.3	4.5	7.9	8.4	9.0	10.1	9.4	8.0
CaO	10.3	10.8	9.9	10.7	9.7	9.1	9.8	10.3
Na_2O	0.39	0.51	0.36	0.38	0.38	0.36	0.34	0.42
K_2O	0.06	0.12	0.06	0.06	0.06	0.09	0.05	0.06
MG#	44.4	29.8	41.4	44.2	46.0	48.0	46.6	42.6
Sc	84	71	82	85	81	80	87	82
V	108	18	105	106	131	143	154	102
Cr	3090	850	3210	3080	3350	3870	3740	2760
Co	20.2	12.3	21.6	19.7	21.5	23.2	20.3	18.5
Ni	22	20	11	13	14	7	12	19
Sr	240	170	220	230	200	160	---	200
Cs	0.12	0.28	0.07	0.10	0.09	0.15	0.11	0.04
Ba	148	160	66	101	128	64	91	56

TABLE 3: Cont.

SAMPLE TYPE	71088,5 A	71095,0 A	71096,5 A	74286,4 A	75065,0 A	75086,4 A	75087,4 A	79265,5 A
Wt (g)	0.3312	0.7839	0.5992	0.5660	0.9090	0.5067	0.5458	0.3852
La	6.2	10.7	6.1	6.1	5.2	5.8	5.8	6.6
Ce	28	41	26	24	20	26	24	29
Nd	30	40	23	24	20	25	22	30
Sm	9.4	15.3	9.1	9.1	7.7	8.6	8.9	9.7
Eu	2.0	3.1	2.0	2.0	1.8	1.9	1.7	2.0
Tb	2.7	4.2	2.5	2.5	2.1	2.5	2.4	2.6
Dy	20.0	28.1	18.2	18.4	15.2	17.0	17.1	18.6
Yb	9.2	14.3	8.8	8.9	7.7	8.5	8.8	9.7
Lu	1.34	2.06	1.30	1.28	1.14	1.22	1.25	1.36
Zr	250	300	150	210	120	150	240	240
Hf	9.0	12.9	8.5	8.5	7.4	8.1	8.1	8.4
Ta	1.8	2.3	1.7	1.6	1.6	1.6	1.6	1.6
Th	0.3	0.6	0.1	---	0.3	0.2	0.1	0.3
U	---	0.4	0.2	0.2	0.2	0.2	0.2	0.2
La/Sm	0.656	0.703	0.674	0.671	0.667	0.667	0.656	0.681
Cr/La	499	79	524	502	650	673	649	419

TABLE 3: Cont.

SAMPLE TYPE	70139,4 B1	70148,0 B1	70155,0 B1	70156,0 B1	70157,0 B1	71047,4 B1	71089,0 B1	71097,4 B2	71157,5 B2
Wt (g)	0.5525	0.5620	0.4207	0.2310	0.3086	0.6921	0.7996	0.3525	0.4120
TiO_2	13.1	12.5	12.4	13.4	13.4	12.9	11.3	12.0	12.6
Al_2O_3	8.3	8.1	10.2	9.5	9.8	8.5	9.2	8.9	8.5
FeO	17.6	18.2	17.2	18.0	17.1	17.8	17.6	19.6	19.5
MnO	0.232	0.237	0.232	0.239	0.237	0.238	0.245	0.259	0.259
MgO	9.6	8.8	8.7	9.8	9.1	8.8	6.5	7.1	7.5
CaO	10.0	9.7	9.6	10.5	11.1	9.8	10.7	10.8	10.7
Na_2O	0.36	0.36	0.44	0.39	0.44	0.39	0.43	0.42	0.36
K_2O	0.04	0.05	0.03	0.05	0.06	0.04	0.06	0.06	0.03
MG#	49.3	46.3	47.4	49.2	48.7	46.8	39.7	39.2	40.7
Sc	80	79	72	82	77	78	79	90	86
V	143	132	130	149	136	132	65	74	114
Cr	3810	3720	3380	3910	3670	3660	2290	2270	2650
Co	26.2	21.6	21.3	21.6	19.3	24.0	18.7	20.2	21.5
Ni	31	9	78	42	39	13	14	51	30
Sr	180	170	210	170	130	180	220	140	110
Cs	0.02	0.11	0.11	0.16	0.12	0.16	0.09	0.24	0.06
Ba	67	67	35	65	82	53	76	76	82
La	3.1	3.7	3.0	3.1	4.4	4.5	4.3	6.4	5.2
Ce	13	16	12	14	16	19	16	24	18
Nd	15	14	13	14	18	17	16	23	21
Sm	4.8	5.6	4.8	5.2	6.8	6.7	6.7	7.6	6.2
Eu	1.4	1.6	1.7	1.5	1.9	1.7	1.8	1.6	1.4
Tb	1.5	1.5	1.7	1.6	1.9	2.0	2.0	2.2	1.7
Dy	9.7	11.2	10.5	11.3	13.4	14.1	13.9	14.6	12.6
Yb	5.4	6.1	5.3	5.6	6.8	6.6	6.9	7.7	6.8
Lu	0.81	0.92	0.78	0.85	0.99	1.00	1.03	1.15	1.00
Zr	160	110	130	---	170	170	150	110	90
Hf	5.7	6.2	5.4	5.6	6.7	6.5	6.3	6.9	6.4
Ta	1.2	1.4	1.2	1.2	1.4	1.3	1.5	1.5	1.5
Th	0.3	0.1	0.1	0.1	0.2	0.2	0.3	0.3	0.5
U	0.1	0.3	0.2	0.1	---	0.2	0.2	0.1	---
La/Sm	0.638	0.663	0.620	0.598	0.651	0.671	0.644	0.840	0.833
Cr/La	1249	1011	1146	1249	832	821	528	357	510

in each of the types defined by whole-rock composition. We have used the chemical criteria of RHODES et al. (1976) and WARNER et al. (1979) to divide our basalts into A and B types (see Introduction). Of our 25 basalts, 16 are of Type A, 9 are of Type B, and 0 are of Type C (Table 3). Distinctions between the REE contents are highlighted in Fig. 3. All the basalts are LREE depleted and exhibit negative Eu anomalies. It appears that on the basis of REEs, the new variant of Apollo 17 high-Ti basalt (70091,2161) reported by RYDER (1988) may be a Type B high-Ti basalt. However, the MgO, Cr_2O_3, and TiO_2 indicate that 70091,2161 is a separate type of Apollo 17 high-Ti basalt, termed "Type D" by RYDER (1990). The reported REE profile for 70091,2161 overlaps the lower end of our Type B basalts (Fig. 3), but has a distinctly deeper Eu anomaly.

WARNER et al. (1979) presented Apollo 17 high-Ti basalt data on a La/Sm versus La plot, and demonstrated that the Type A's exhibited little variation in La/Sm ratio, whereas the Type B's exhibited a range in La/Sm ratio. These authors concluded that in order to achieve the observed range of La/Sm ratio in Type B high-Ti basalts, magmas were derived from variations in the degree of partial melting. On the other hand, Type A high-Ti basalts were generated from a common parental magma by fractional crystallization of observed phenocryst phases; this process does not radically alter the La/Sm ratio.

In Fig. 4, we have presented our new data on a La/Sm versus La plot with all previously reported Type A and B high-Ti basalt compositions. These new data fall within and extend the ranges of previously defined A and B basalts. The nature of the trends defined by Type A and B led NEAL et al. (1989a) to conclude that both types had a common parent, but underwent different post-magma-generation evolution. Also plotted on this diagram is the error bar associated with the La/Sm ratio. Although calculation of element-element ratios magnifies the error associated with the determination of the element, this does not explain all of the range observed in the La/Sm ratio of the Apollo 17 high-Ti basalts.

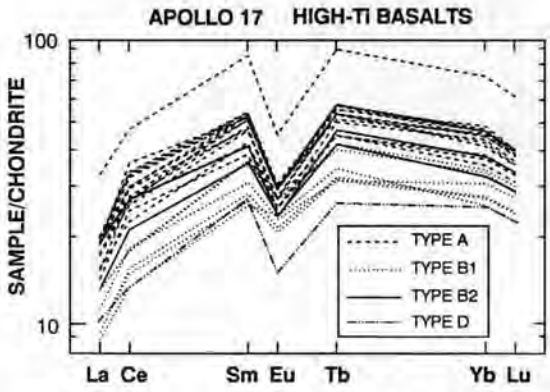

FIG. 3. REE patterns determined by INAA from the 25 "new" Apollo 17 high-Ti basalts described in this study and the new "Type D" Apollo 17 high-Ti basalt described by RYDER (1988). Although this falls within our range of Type B1 high-Ti basalts, it possesses a distinctly deeper negative Eu anomaly and unique trace element signature.

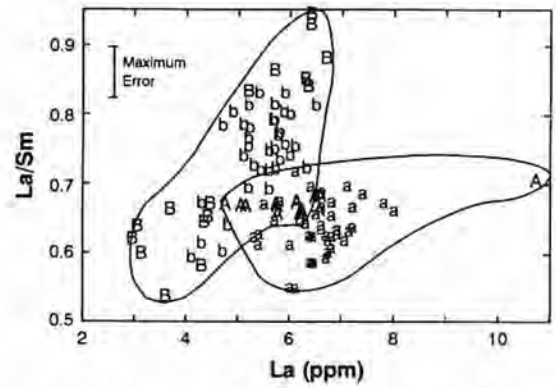

FIG. 4. All Apollo 17 high-Ti basalt data for Type A and B varieties represented on a La (ppm) vs. La/Sm plot. Capital letters represent data from this study; those of lower case represent data previously published. Only two "b's" plot in the Aa field.

DISCUSSION

We have argued above that our analyses represent whole-rock compositions. However, it is possible that some of the "new" Apollo 17 basalts are cumulates, especially as many of these are coarse-grained plagioclase-poikilitic varieties. Therefore, before modeling of Apollo 17 high-Ti basalt petrogenesis can be undertaken, we must first demonstrate that the samples analyzed represent liquid compositions. MURALI et al. (1977) and WARNER et al. (1977) concluded that basalt 71597 was a product of partial olivine accumulation. This conclusion was based on the high MgO content, high modal olivine, and a discrepancy between observed and calculated Fo contents (Table 4).

Following the method of MURALI et al. (1977) and WARNER et al. (1977), we have calculated the expected Fo contents of olivines for the new Apollo 17 high-Ti basalts on the basis of equilibrium partitioning of Mg and Fe between olivine and liquid. We assume that the whole-rock data represents liquid compositions and present results in Table 4. The olivine Kd's used for Fe-Mg partitioning were calculated from the equation derived by DELANO (1980). These fall within 0.26 to 0.29, spanning the range of olivine Kd's measured in high-Ti basalts (LONGHI et al., 1978). The whole-rock MgO contents and modal olivine in each of these basalts are also given in Table 4. All of the "new" basalts possess lower MgO contents and modal % olivine than 71597 (MURALI et al., 1977; WARNER et al., 1977). However, observed olivine Fo contents are similar to those of 71597. Furthermore, these observed Fo contents are all, with two exceptions (71097 and 71157), below calculated values.

Results of these calculations would appear to suggest that the majority of our new Apollo 17 high-Ti basalts are cumulates. According to WARNER et al. (1977), if olivine accumulation has occurred, one would expect to observe olivines with lower Fo contents than calculated from whole-rock analyses, coupled with a high olivine modal abundance and high bulk rock MgO contents. It is difficult to distinguish, on the basis of composition alone, between olivines which grew and equilibrated in a closed system and those which

TABLE 4: Comparison of observed and calculated Fo contents of olivines in the 25 "new" Apollo 17 high-Ti basalts. The olivine/liquid Kd's determined by theequation of DELANO (1980) for high-Ti lunar basalts have been used in these calculations. The cumulate 71597 (WARNER et al., 1977) is included for comparison.

SAMPLE	TYPE	MODAL OLIVINE	OBSERVED Fo	WHOLE-ROCK MgO	WHOLE-ROCK MG#	CALCULATED Fo
70138	A	3.0	48-69	8.2	44.9	75.3
70145	A	1.9	60-73	8.5	44.4	75.2
70146	A	2.1	66-68	8.8	44.4	75.1
70147	A	0.0	---	8.8	46.7	---
70165	A	0.9	49-64	8.7	46.4	76.4
71048	A	7.6	63-66	8.0	43.8	74.6
71049	A	0.2	57-67	8.3	45.4	75.6
71087	A	0.2	58-71	7.9	42.8	73.8
71088	A	8.2	43-71	8.3	44.4	74.9
71095	A	0.0	---	4.5	29.8	---
71096	A	7.1	57-70	7.9	41.4	72.7
74286	A	2.1	63-71	8.4	44.2	74.6
75065	A	1.0	65-70	9.0	46.0	76.2
75086	A	1.3	58-67	10.1	48.0	77.5
75087	A	0.4	37-65	9.4	46.6	76.8
79265	A	1.0	51-68	8.0	42.6	73.2
70139	B1	2.5	55-69	9.6	49.3	78.6
70148	B1	1.0	63-66	8.8	46.3	76.3
70155	B1	1.9	58-67	8.7	47.4	77.0
70156	B1	2.3	68-70	9.8	49.2	78.7
70157	B1	0.4	62-70	9.1	48.7	78.3
71047	B1	1.1	49-73	8.8	46.8	76.8
71089	B1	0.3	55-67	6.5	39.7	70.5
71097	B2	6.8	60-72	7.1	39.2	70.4
71157	B2	2.7	63-75	7.5	40.7	71.9
71597	--	*19.3*	*63-75*	*15.8*	*58.7*	*85.2*

were accumulated into a fractionating melt. The criterion of observed versus calculated olivine Fo contents must be coupled with *high modal abundance of olivine* and *high MgO contents*. While the olivine compositions (Table 4) are ambiguous, bulk rock MgO contents are within the range defined by previous workers for fine-grained (non-cumulate) high-Ti basalts, and modal olivine is low. The highest bulk rock MgO is 10.1 wt%, which is much lower than the 15.8 wt% MgO reported in 71597. WARNER et al. (1977) concluded that 24–27% olivine accumulation had occurred in 71597. When this amount of olivine is subtracted, the bulk rock MgO is reduced to 9–11 wt%, similar to that observed in our samples. Therefore, we suggest that our new basalt data are representative of liquid rather than cumulate compositions.

In order to evaluate thoroughly the petrogenesis of Apollo 17 Type A and B high-Ti basalts, we will plot all available data for these basalts on all diagrams. Data sources are BRUNFELT et al. (1974), WARNER et al. (1975, 1979), SHIH et al. (1975), RHODES et al. (1976), and MURALI et al. (1977). The previous data include only basalts which are considered to represent liquid compositions. This combination of data on these plots allows previous models of Apollo 17 basalt petrogenesis to be evaluated.

Re-Examination of Previous Petrogenetic Models

WARNER et al. (1979) proposed that, due to variations of the La/Sm ratio, Type B basalts could be modeled by varying the degree of partial melting of the source. However, when the Cr/La ratio (used as a fractionation index) is plotted against Hf (ppm) for all Type A and B data (Fig. 5), the Type B high-Ti basalts contain approximately constant Hf abundances (5.5–7.8 ppm), whereas the Type A's exhibit variable Hf abundances from 7 to 13 ppm. If variable degrees of partial melting were responsible for the compositional variations observed in the Type B basalts, Hf would also vary (i.e., higher Hf ppm in a small partial melt, lower Hf ppm in a large partial melt). The only way to generate the Type B trend in Fig. 5 by partial melting is for significant ilmenite (or armalcolite) to be left as a residual phase, as this would buffer the Hf content of the magma. Such a scenario is unlikely

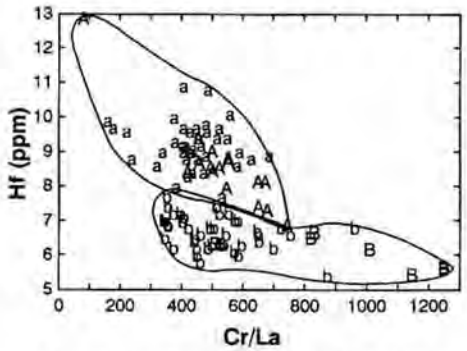

FIG. 5. All Apollo 17 high-Ti basalt data for Type A and B varieties represented on a Cr/La vs. Hf (ppm) plot. Capital letters represent data from this study; those of lower case represent data previously published.

considering the high and variable abundance of Ti in these basalts, the low postulated ilmenite abundance in the Apollo 17 high-Ti basalt source (3% maximum—UNRUH et al., 1984), and experimental work (e.g., GREEN et al., 1975) which indicates that ilmenite was not a residual phase after partial melting. Therefore, we do not agree with the hypothesis of WARNER et al. (1979).

Incorporation of an Apollo 17 KREEPy component (Apollo 17 KREEP compositions from RYDER et al., 1977; SALPAS et al., 1987) into a parental magma by AFC has been proposed by NEAL et al. (1989b) to generate the observed increase in La/Sm ratio in Type B basalts. However, all are LREE depleted (Fig. 3) and will require only minor amounts of KREEP to generate observed La/Sm ratios. Modeling of the compatible elements, indicates that a model of KREEP assimilation by a fractionating Type B parental magma is incapable of reproducing the observed ranges of both compatible and incompatible elements in Type B basalt compositions.

Generation of the Apollo 17, Type A, high-Ti basalts was previously modeled by fractional crystallization of observed phenocryst phases (e.g., RHODES et al., 1976; WARNER et al., 1979). However, this modeling was conducted in a somewhat qualitative sense, in that only a small number of elements were used and the fractionating assemblage was not varied as crystallization proceeded. The fact that armalcolite is generally mantled by ilmenite and olivine by pyroxene demonstrates the evolution of the fractionating assemblage.

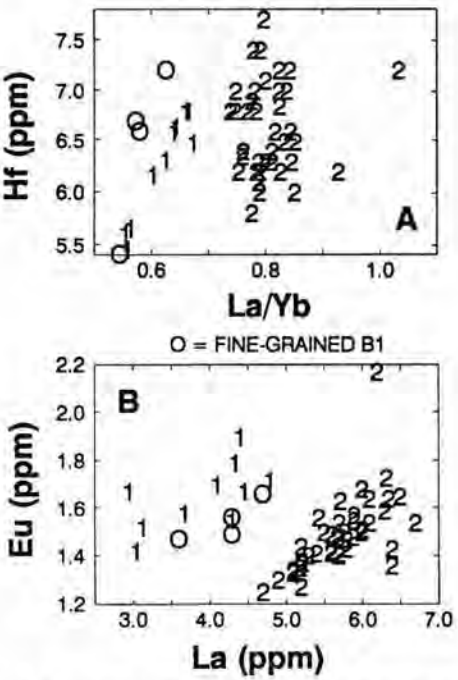

FIG. 6. Splitting of the Type B Apollo 17 high-Ti basalts into two groups—B1 and B2. The symbol "O" represents fine-grained B1 basalts, demonstrating that this grouping is not a product of sampling errors.

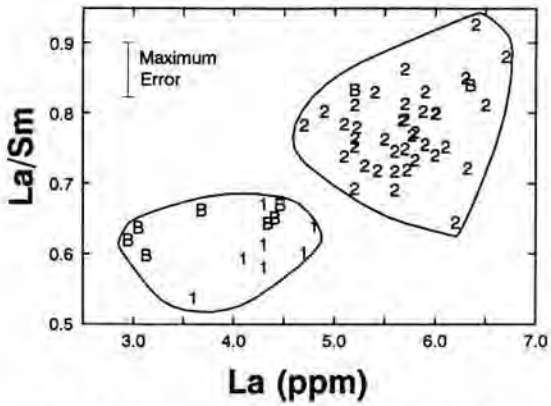

FIG. 7. A plot of La (ppm) vs. La/Sm depicting two groups of Type B basalts. Numbers represent previously published data; letters represent data from this study.

Type B Basalts—*One* Type, *Two* Groups

During the present investigation we discovered that, although Type B basalts form a continuum on already published plots, two groups actually exist. The La/Yb ratio is

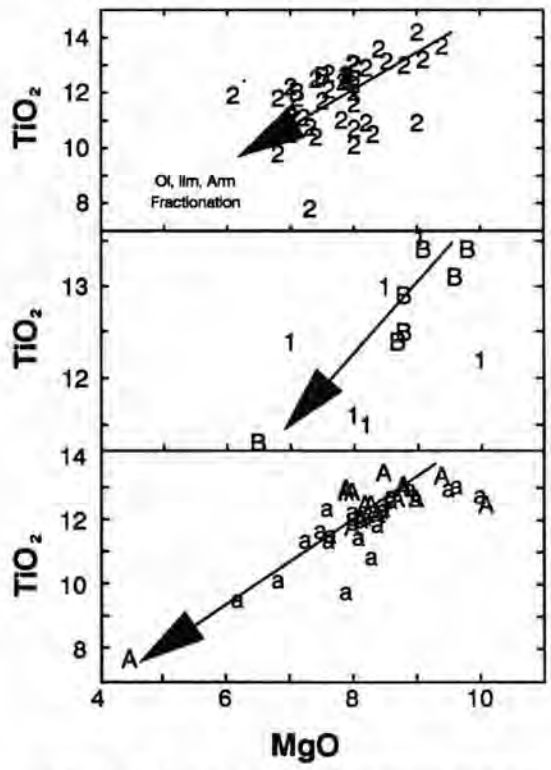

FIG. 8. MgO vs. TiO_2 plots depicting major element trends indicative of olivine and FeTi-oxide fractionation in Type A, B1, and B2 Apollo 17 high-Ti basalts. Numbers and lower-case letters represent previously published data; capital letters represent data from this study.

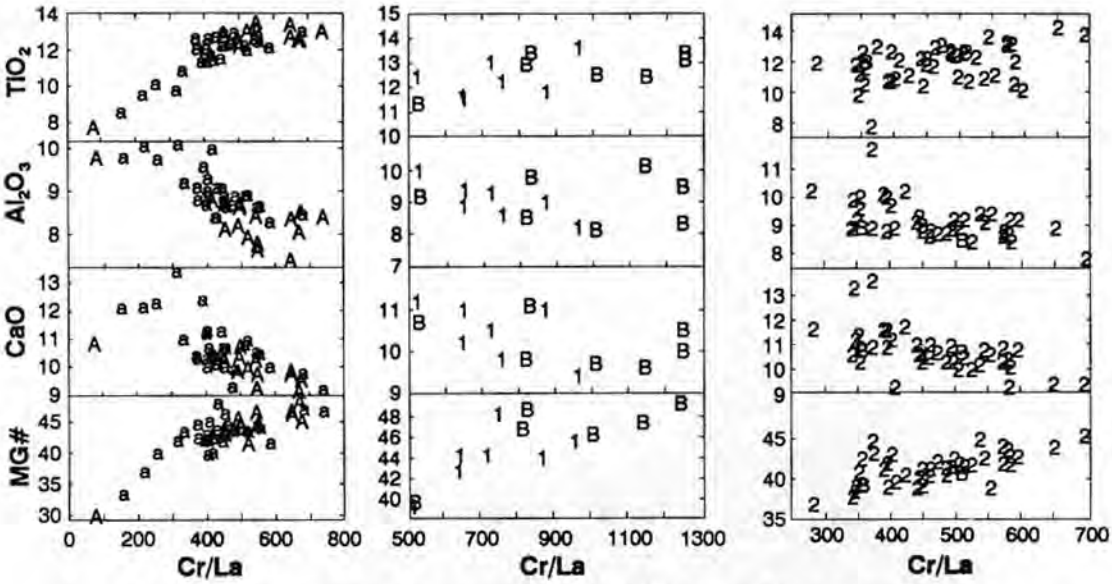

FIG. 9. Major elements plotted against the fractionation index of Cr/La ratio for all Type A, B1, and B2 Apollo 17 high-Ti basalts. Numbers represent previously published data; letters represent data from this study.

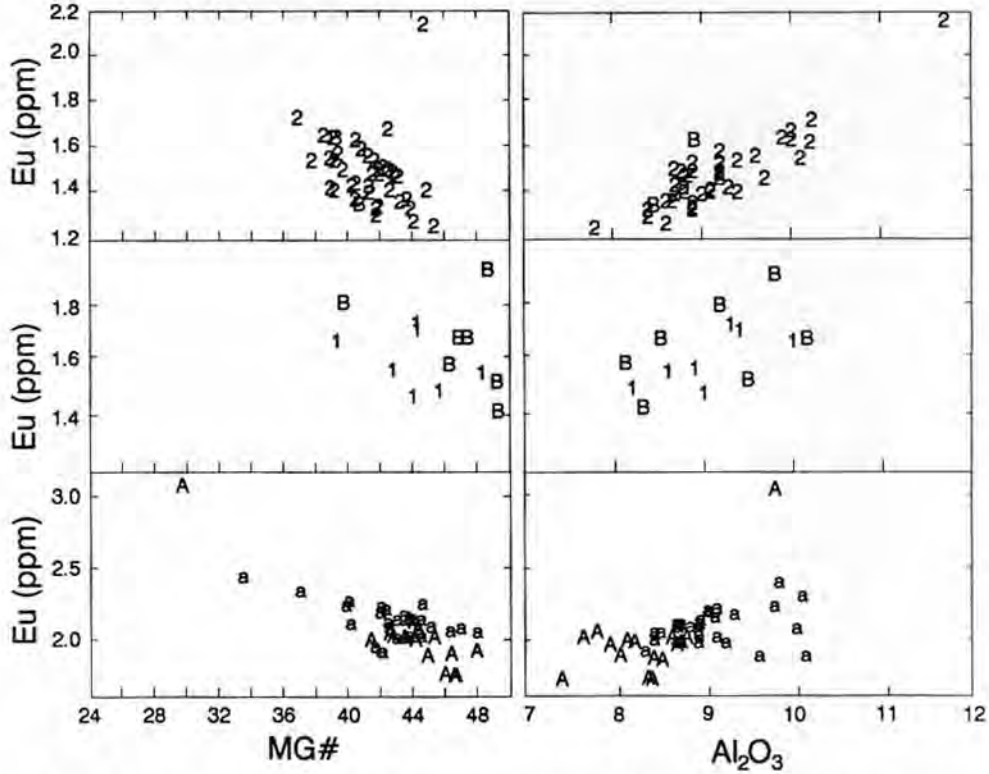

FIG. 10. MG# and Al_2O_3 plotted against Eu (ppm) for Type A, B1, and B2 Apollo 17 high-Ti basalts demonstrating that plagioclase was not a major liquidus phase during the fractionation of these basalts. Numbers and lower-case letters represent previously published data; capital letters represent data from this study.

plotted against Hf (Fig. 6a) and La against Eu (Fig. 6b) for Apollo 17 Type B basalts only. Two distinct groups are portrayed, especially as depicted on a plot of La versus Eu (Fig. 6b). A distinct break in La/Yb ratio at 0.7 is observed in the Type B basalt suite (Fig. 6a). We consider that these are the definitive plots for the identification of *Type B1 and B2*.

Most of the basalts which define Group B1 (10 out of 14) are coarse-grained (Tables 1 and 3) with 12 of these being from this study. Such an observation raises the possibility that these are cumulates. However, four fine-grained variants of B1 basalts exist and practically span the entire B1 range (Fig. 6a,b). Therefore, this observation coupled with the olivine discussion above demonstrates that the definition of Group B1 is not an artifact of mineral accumulation.

Correlations defined in Fig. 6 are generally parallel, though offset, making it extremely difficult to generate one from the other by assimilation, fractionation, periodic magma replenishment, or a combination of these processes. When La is plotted against the compatible and major elements, a continuum is again witnessed. We interpret that these two Type B basalt types were derived from two distinct source regions, similar in compatible and major element characteristics, but containing different absolute abundances of the REE and high field strength (HFS) elements. The observation that the trends for Apollo 17 Type B1 and B2 high-Ti basalts are parallel suggest they experienced similar post-magma-generation processes.

MODELING

With the recognition of Apollo 17 Type B1 and B2 distinct magma types, the need for the generation of a range of La/Sm ratios is radically reduced. Figure 7 depicts La versus La/Sm for the Type B basalts. Two distinct groups are present, each with a limited range of La/Sm ratio. The Type B1 basalts exhibit a range of La/Sm ratio of ~0.1 and the Type B2's ~ 0.2. As stated earlier, much of the scatter of these data may be due to the magnification of the analytical errors in the calculation of such ratios. The maximum error in La/Sm ratio (~0.08) is shown by the error bar in Fig. 7.

This observation, coupled with the relatively flat trend of the Type A basalts on such a plot (Fig. 4) and the inadequacy of previous models (see above), allows us to model the compositional variation of each basalt type by fractional crystallization. Further evidence of fractional crystallization affecting both the Type A and B basalts can be seen by plotting MgO against TiO_2 for Type A, B1, and B2 basalts (Fig. 8). Gen-

TABLE 5: Modeling Parameters.

Partition Coefficients:

	OLIVINE	ARMALCOLITE	ILMENITE	SPINEL	CPX
Cr	0.7	(3.5)	6	51	1
Co	2.5	2.2	2.2	2.8	1.2
La	0.0064	0.006	0.029	0.01	0.058
Sm	0.0066	0.008	0.053	0.0064	0.45
Eu	0.0068	0.006	0.02	0.0061	0.48
Yb	0.02	0.07	0.39	0.76	0.58
Hf	0.04	1.47	0.42	0.1	0.26

References: () = estimated from STANIN and TAYLOR (1980); AKELLA et al. (1976); BIRD (1971); DOSTAL et al. (1983); HASKIN and KOROTEV (1977); IRVING (1978); IRVING and FREY (1984); IRVING et al. (1978); LINDSTROM (1976); McKAY et al. (1986); NAGASAWA et al. (1976, 1980); PASTER et al. (1974); RAY et al. (1983).

Proportions of Fractionating Phases (%):

	TYPE A			TYPE B1			TYPE B2		
F	0-10	10-40	>40	0-10	10-20	>20	0-10	10-20	>20
Ol	93	78	0	89	85	0	84	70	0
Armal	5	0	0	10	0	0	15	0	0
Spinel	2	2	0	1	0	0	1	0	0
Ilm	0	20	40	0	15	30	0	30	40
Cpx	0	0	60	0	0	70	0	0	60

Estimated Parental Compositions (ppm):

	TYPE A	TYPE B1	TYPE B2
Cr	4100	4300	3300
Co	28	30	27
La	4.8	2.8	4.4
Sm	7.0	4.8	5.8
Eu	1.55	1.20	1.20
Yb	7.1	5.1	5.9
Hf	6.8	5.1	5.8
La/Sm	0.679	0.589	0.759
Cr/La	860	1540	750

erally, negative correlations are observed in each case, which conform with olivine, ilmenite, and armalcolite fractionation.

In our modeling, we have used the Cr/La ratio rather than MG# as a fractionation index because these elements are more accurately determined than by INAA. We are confident that the high Cr/La ratios observed in the new, coarse-grained, Apollo 17, high-Ti basalts are not due to Cr-spinel accumulation. As noted in petrography, most spinel phases are found as inclusions in olivine or in pyroxene after olivine, suggesting that these crystallized almost simultaneously. We have argued above that olivine accumulation has not occurred in our samples and by inference neither has Cr-spinel accumulation.

As fractional crystallization proceeds, Cr/La in the residual magma decreases. Our model uses petrographic as well as geochemical observations in order to determine the fractionating phases. In Fig. 9, TiO_2, Al_2O_3, CaO, and MG# are plotted against the Cr/La ratio for the Type A, B1, and B2 high-Ti basalts. Trends are similar for all the basalt types. Generally, as the Cr/La ratio decreases, MG# and TiO_2 decrease and CaO and Al_2O_3 increase. There is possibly a slight decrease in CaO towards the lower end of the correlation in the Type A's, but this is not definitive.

The removal of observed phenocryst phases (olivine, Cr-ulvöspinel, armalcolite, ilmenite, and pyroxene) can adequately generate the trends in Fig. 9. The steady increase of CaO and Al_2O_3 with decreasing Cr/La ratio indicates that pyroxene was a relatively late-stage fractionating phase and that plagioclase was never a liquidus phase in the evolution of these basalts. This is supported by Fig. 10. Here, MG# and Al_2O_3 are plotted against Eu abundance for Type A, B1, and B2 basalts. The Eu abundance in each basalt type increases with decreasing MG# and increasing Al_2O_3 contents.

Proportions of the fractionating phases were estimated from petrography, as was the relative timing of their crystallization. During the first 10% crystallization, olivine, armalcolite, and Cr-ulvöspinel were liquidus phases. During the next 10% (or 30% in the case of the Type A basalts), ilmenite replaced armalcolite. Above 20% (or 40% for the Type A's), pyroxene and ilmenite were the only fractionating phases. Partition coefficients with data sources and proportions of fractionating phases are presented in Table 5. These partition coefficients were kept constant throughout the modeling of the Type A, B1, and B2 basalts (Table 5).

The existing suite of Apollo 17 high-Ti basalts does not yield any likely parental compositions to Types A, B1, and

TABLE 6: Modeling Results (ppm):

TYPE A: % Cryst.	10	20	30	40	50	60	70	80
Cr	3750	3110	2530	2000	1620	1280	980	720
Co	24.0	20.5	17.3	14.3	13.4	12.5	11.5	10.5
La	5.3	5.9	6.6	7.5	8.3	9.3	10.6	12.2
Sm	7.8	8.6	9.7	11.0	11.9	12.9	14.2	15.9
Eu	1.72	1.91	2.15	2.45	2.64	2.87	3.15	3.51
Yb	7.9	8.7	9.6	10.9	11.5	12.2	13.0	14.0
Hf	7.5	8.2	9.1	10.2	11.0	11.9	13.0	14.5
La/Sm	0.679	0.679	0.679	0.680	0.698	0.718	0.742	0.770
Cr/La	710	530	385	270	195	140	93	59

TYPE B1: % Cryst.	10	20	30	40	50
Cr	4090	3880	3310	2780	2270
Co	26.0	22.2	20.9	19.7	18.4
La	3.1	3.5	3.8	4.3	4.8
Sm	5.3	5.9	6.3	6.8	7.4
Eu	1.33	1.48	1.59	1.71	1.87
Yb	5.6	6.2	6.5	6.9	7.3
Hf	5.5	6.0	6.5	7.0	7.7
La/Sm	0.589	0.590	0.607	0.628	0.652
Cr/La	1310	1120	870	650	470

TYPE B2: % Cryst.	10	20	30	40
Cr	3090	2700	2190	1730
Co	23.2	20.0	18.7	17.5
La	4.9	5.4	6.0	6.7
Sm	6.4	7.1	7.7	8.4
Eu	1.33	1.48	1.59	1.73
Yb	6.5	7.1	7.5	7.9
Hf	6.2	6.7	7.5	8.0
La/Sm	0.759	0.759	0.779	0.802
Cr/La	633	498	365	257

B2. The most primitive examples (with regard to Cr/La ratio) have either a coarse-grained plagioclase-poikilitic or porphyritic texture, demonstrating that these have already experienced a degree of fractionation. Therefore, we used element-element plots to estimate parental compositions for the three basalt types. However, although the choice of a parental composition is somewhat subjective and model dependent, the parents thus calculated are reasonable in that they are LREE depleted, and depleted in incompatible element and enriched in compatible element abundances relative to the observed Apollo 17 basalts (Table 5) and possess a MG# in the range 49–51.

Results

The results of our modeling are presented in Figs. 11–13 and Table 6. The Cr/La ratio is plotted against Cr, Co, La, Sm, Eu, Yb, and Hf (ppm), along with the calculated fractional crystallization path. We have chosen these elements in order to model compatible, rare earth (light, middle, and heavy), and the high field strength (HFS) elements. Although Ni is more sensitive to olivine and opaque mineral crystallization than Co, it was not used in our modeling due to the large errors associated with the Ni INA analyses. In all plots, the calculated fractionation paths can adequately model the observed compositional ranges. The scatter observed in Figs. 11–13 may be the result of sampling errors or other magmatic processes affecting the systems, such as magma replenishment/mixing. Furthermore, analytical errors may also be a contributing factor as they are magnified when element-element ratios are calculated.

The fractionating phases were varied as crystallization proceeded, consistent with the petrographic observations (see above and Table 6). For example, the majority of the Type A high-Ti basalts are generated after 40% fractional crystallization in all plots (Fig. 11). Two previously analyzed Type A basalts extend up to 60% crystallization, but one of our new basalts is only generated after 70–80% (Fig. 11). This sample is 71095, and although classified as a Type A high-Ti basalts, it is petrographically and mineralogically distinct; 71095 is the only example of a Type II, Apollo 11, low-K-type, high-Ti basalt in our new basalt suite. It could be that these basalts are produced after extreme fractionation (70–80%) of a Type A parent, or they originated from their own parent which fortuitously falls along the Type A evolution path. On the basis of the present data set, such questions cannot be resolved.

The Type B1 and B2 basalts (Figs. 12 and 13) have been similarly modeled, and the compositional ranges require 50% and 40% fractional crystallization, respectively. As with the Type A's, the calculated fractional crystallization paths for the Type B1 and B2 high-Ti basalts adequately model all data. The amount of fractional crystallization required in our modeling is considerably greater than the 4–22% reported by RHODES et al. (1976), because the present much larger data set shows a wider compositional range.

The effect of fractional crystallization upon the MG# is moderate (Fig. 9). In the Type A, B1, and B2 suites, MG# varies from 27–49, 39–49, and 36–45, respectively. Although the proposed maximum amounts of fractional crystallization are large (up to 80% in the Type A's), the change in the MG# would not be dramatic. This is due to the nature of the fractionating assemblage; both Mg- (silicate) and Fe-rich (oxide) phases are being crystallized. Where this process occurs is beyond the scope of this paper, but it is likely that a holding chamber was present either in the lower crust or at the crust-mantle boundary. The presence of phenocrysts in these high-Ti basalts demonstrates a period of cooling prior to extrusion.

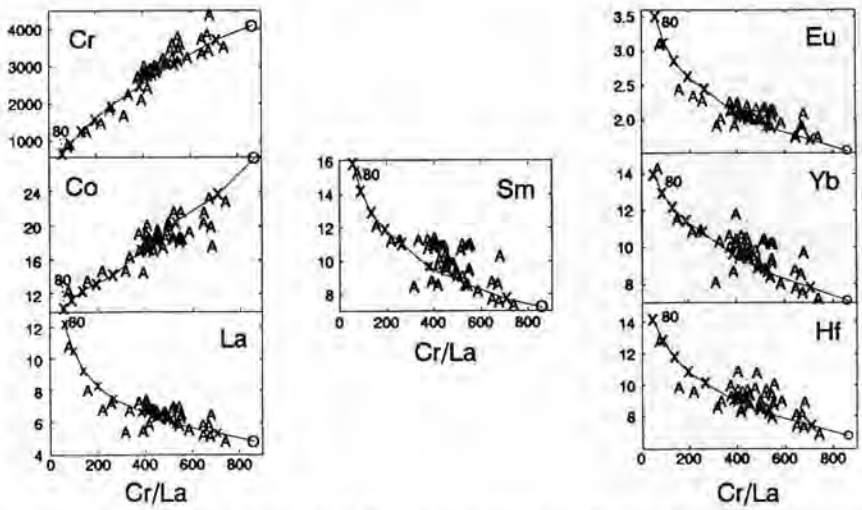

FIG. 11. Modeling of all Type A Apollo 17 high-Ti basalts by fractional crystallization of observed phenocryst phases. The open circle represents the calculated parental magma composition and tick marks are in 10% increments. All data can be generated after 70–80% fractional crystallization, but the majority of the basalts are generated after 40–50% fractional crystallization.

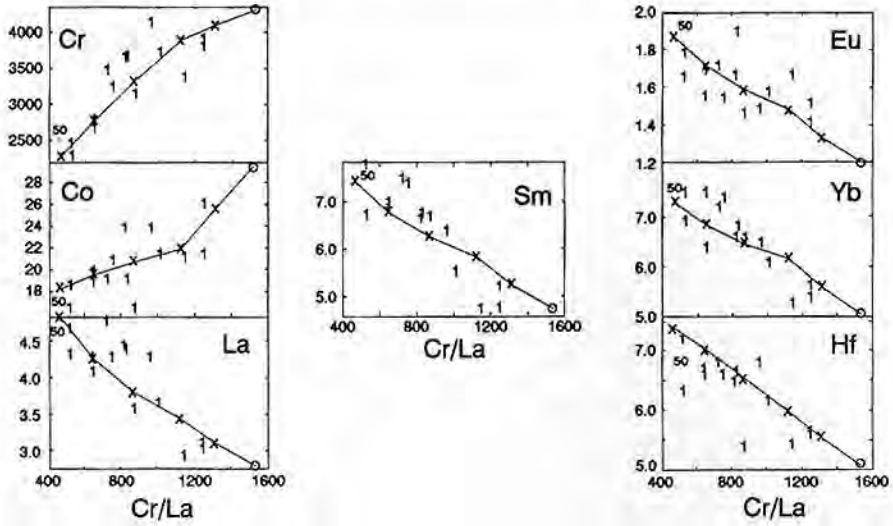

FIG. 12. Modeling of all Type B1 Apollo 17 high-Ti basalts by fractional crystallization of observed phenocryst phases. The open circle represents the calculated parental magma composition and tick marks are in 10% increments. All data can be generated after 50% fractional crystallization.

SUMMARY

The classification of the Apollo 17 high-Ti basalts on the basis of petrography does not conform with that on the basis of whole-rock geochemistry; from our data Type 1A and 1B textures are found in Type B basalts, and all textures are found in the Type A variety. The inclusion of our 25 new Apollo 17 high-Ti basalts in the data set has identified two groups of Type B basalts. Type B1 contains lower REE and HFS element abundances, and a lower La/Sm ratio than the Type B2's. We conclude that the Type A, B1, and B2 basalts were produced from source regions of similar major- and compatible-element abundances, but distinct incompatible distributions.

The Type A, B1, and B2 basalts define trends on element versus fractionation index plots. The Cr/La ratio rather than

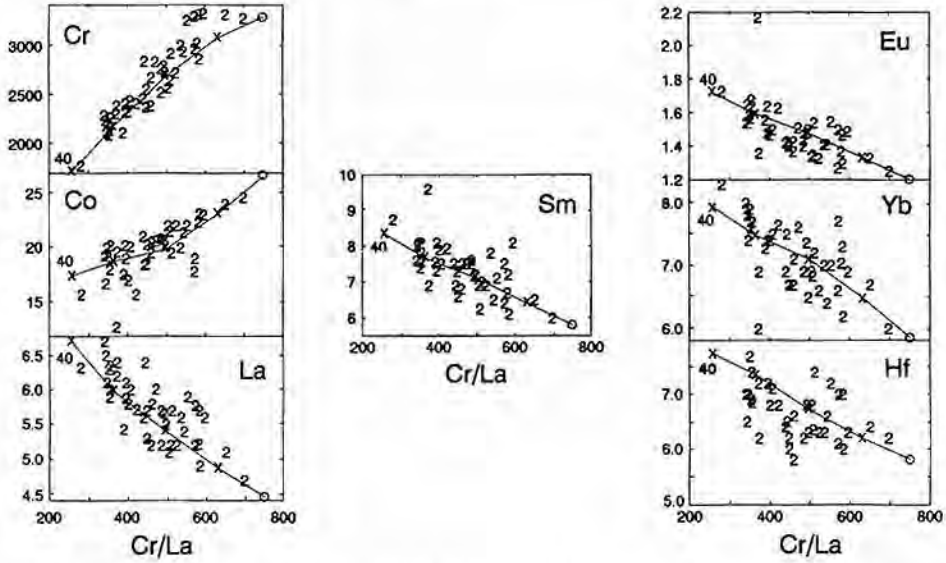

FIG. 13. Modeling of all Type B2 Apollo 17 high-Ti basalts by fractional crystallization of observed phenocryst phases. The open circle represents the calculated parental magma composition and tick marks are in 10% increments. All data can be generated after 40% fractional crystallization.

MG# was chosen as the fractionation index because these elements are measured more accurately by INAA than are Mg and Fe. *The compositional ranges of all Apollo 17 high-Ti basalt types can be adequately generated by the fractional crystallization of observed phenocryst phases.* Plagioclase fractionation was never involved in this process. The fractionating assemblage was deduced from petrographic observations and parental compositions were estimated from element-element plots.

Acknowledgments—This paper has greatly benefited from stimulating discussions with Dr. James B. Pačes. Thoughtful reviews by Graham Ryder, John Delano, Jeff Taylor, and Gordon McKay have improved the quality of this manuscript. Support for this research was through NASA grants NAG 9-62 to L.A.T. and NAG 9-63 to R.A.S.

Editorial handling: G. A. McKay

REFERENCES

AKELLA J., WILLIAMS R. J., and MULLINS O. (1976) Solubility of Cr, Ti, and Al in coexisting olivine, spinel, and liquid at 1 atmosphere. *Proc. Lunar Sci. Conf. 7th,* 1179–1194.

BROWN G. M., PECKETT A., EMELEUS C. H., PHILLIPS R., and PINSENT R. H. (1975) Petrology and mineralogy of Apollo 17 mare basalts. *Proc. Lunar Sci. Conf. 6th,* 1–13.

BRUNFELT A. O., HEIER K. S., NILSSEN B., STEINNES E., and SUNDVOLL B. (1974) Elemental composition of Apollo 17 fines and rocks. *Proc. Lunar Sci. Conf. 5th,* 981–990.

DELANO J. W. (1980) Chemistry and liquidus phase relations of Apollo 15 red glass: Implications for the deep lunar interior. *Proc. Lunar Planet. Sci. Conf. 11th,* 251–288.

DOSTAL J., DUPUY C., CARRON J. P., LE GUEN DE KENNEIZON M., and MAURY R. C. (1983) Partition coefficients of trace elements: applications to the volcanic rocks of St Vincent, West Indies. *Geochim. Cosmochim. Acta* **47,** 525–533.

DYMEK R. F., ALBEE A. L., and CHODOS A. A. (1975) Comparative mineralogy and petrology of Apollo 17 mare basalts: Samples 70215, 71055, 74255, and 75055. *Proc. Lunar Sci. Conf. 3rd,* 49–77.

GREEN D. H., RINGWOOD A. E., HIBBERSON W. O., and WARE N. G. (1975) Experimental petrology of Apollo 17 mare basalts. *Proc. Lunar Sci. Conf. 6th,* 871–893.

HASKIN L. A. and KOROTEV R. L. (1977) Test of a model for trace element partition during closed system solidification of a silicate liquid. *Geochim. Cosmochim. Acta* **41,** 921–939.

HESS P. C., RUTHERFORD M. J., GUILLEMETTED R. N., RYERSON F. J., and TUCHDELD H. A. (1975) Residual products of fractional crystallization of lunar magmas: An experimental study. *Proc. Lunar Sci. Conf. 6th,* 893–909.

HUGHES S. S., DELANO J. W., and SCHMITT R. A. (1988) Apollo 15 yellow-brown glass: Chemistry and petrogenetic relations to green volcanic glass and olivine-normative mare basalts. *Geochim. Cosmochim. Acta* **52,** 2379–2391.

IRVING A. J. (1978) A review of experimental studies of crystal-liquid trace element partitioning. *Geochim. Cosmochim. Acta* **42,** 743–747.

IRVING A. J. and FREY F. A. (1984) Trace element abundances in megacrysts and their host basalts: Constraints on partition coefficients and megacryst genesis. *Geochim. Cosmochim. Acta* **48,** 1201–1221.

IRVING A. J., MERRILL R. B., and SINGLETON D. E. (1978) Experimental partitioning of rare earth elements and scandium among armalcolite, ilmenite, olivine, and mare basalt liquid. *Proc. Lunar Planet. Sci. Conf. 9th,* 601–612.

LINDSTROM D. J. (1976) Experimental study of the partitioning of the transition metals between clinopyroxene and co-existing silicate liquids. Ph.D. thesis, Univ. Oregon.

LONGHI J., WALKER D., GROVE T. L., STOLPER E. M., and HAYS J. F. (1974) The petrology of Apollo 17 mare basalts. *Proc. Lunar Sci. Conf. 5th,* 447–469.

LONGHI J., WALKER D., and HAYS J. F. (1978) The distribution of Fe and Mg between olivine and lunar basaltic liquids. *Geochim. Cosmochim. Acta* **42,** 1545–1558.

MCKAY G., WAGSTAFF J., and YANG S.-R. (1986) Zr, Hf, and REE partition co-efficients for ilmenite and other minerals in high-Ti lunar mare basalts: An experimental study. *Proc. Lunar Planet Conf. 17th; J. Geophys. Res.* **91,** D229–D237.

MURALI A. V., MA M.-S., SCHMITT R. A., WARNER R. D., KEIL K., and TAYLOR G. J. (1977) Chemistry of 30 Apollo 17 rake basalts: 71597 a product of partial olivine accumulation (abstr.). *Lunar Sci. VIII,* 703–705.

NAGASAWA H., SCHREIBER H. D., and MORRIS R. V. (1980) Experimental mineral/liquid partition coefficients of the rare earth elements (REE), Sc, and Sr for perovskite, spinel, and melilite. *Earth Planet. Sci. Lett.* **46,** 431–437.

NAGASAWA H., SCHREIBER H. D., and BLANCHARD D. P. (1976) Partition coefficients of REE and Sc in perovskite, melilite, and spinel and their implications for Allende inclusions (abstr.). *Lunar Sci. VII,* 588–590.

NEAL C. R. and TAYLOR L. A. (1989) Metasomatic products of the lunar magma ocean: The role of KREEP dissemination. *Geochim. Cosmochim. Acta* **53,** 529–541.

NEAL C. R., TAYLOR L. A., HUGHES S. S., and SCHMITT R. A. (1989a) Apollo 17 high-Ti basalt petrogenesis: An integrated approach using whole-rock major and trace element analyses (abstr.). *Lunar Planet. Sci. XX,* 776–777.

NEAL C. R., TAYLOR L. A., PATCHEN A. D., and BALLINGTON M. (1989b) Mineralogy and petrography of 28 "new" Apollo 17 basalts (abstr.). *Lunar Planet Sci. XX,* 780–781.

PAPIKE J. J., BENCE A. E., and LINDSLEY D. H. (1974) Mare basalts from the Taurus-Littrow region of the moon. *Proc. Lunar Sci. Conf. 5th,* 471–504.

PASTER T. P., SCHAUWECKER D. S., and HASKIN L. A. (1974) The behavior of some trace elements during solidification of the Skaergaard layered series. *Geochim. Cosmochim. Acta* **38,** 1549–1577.

RAY G. L., SHIMUZU N., and HART S. R. (1983) An ion microprobe study of the partitioning of trace elements between clinopyroxene and liquid in the system diopside-albite-anorthite. *Geochim. Cosmochim. Acta* **47,** 2131–2140.

RHODES J. M., HUBBARD N. J., WIESMANN H., RODGERS K. V., BRANNON J. C., and BANSAL B. M. (1976) Chemistry, classification, and petrogenesis of Apollo 17 mare basalts. *Proc. Lunar Sci. Conf. 7th,* 1467–1489.

RYDER G. (1988) A new variant of high-Ti basalt from the Van Serg drive tube (abstr.). *Lunar Planet. Sci. XIX,* 1013–1014.

RYDER G. (1990) A distinct variant of high-titanium mare basalt from the Van Serg core, Apollo 17 landing site. *Meteoritics* (in press).

RYDER G., STOESER D. B., and WOOD J. A. (1977) Apollo 17 KREEPy basalt: A rock type intermediate between mare and KREEP basalts. *Earth Planet. Sci. Lett.* **35,** 1–13.

RYERSON F. J. and HESS P. C. (1980) The role of P_2O_5 in silicate melts. *Geochim. Cosmochim. Acta* **44,** 611–624.

SALPAS P. A., TAYLOR L. A., and LINDSTROM M. M. (1987) Apollo 17 KREEPy basalts: Evidence for nonuniformity of KREEP. *Proc. Lunar Planet. Sci. Conf. 17th; J. Geophys. Res.* **92,** E340–E348.

SHIH C.-Y., HASKIN L. A., WIESMANN H., BANSAL B. M., and BRANNON J. C. (1975) On the origin of high-Ti mare basalts. *Proc. Lunar Sci. Conf. 6th,* 1255–1285.

SIMON S. B., PAPIKE J. J., SHEARER C. K., HUGHES S. S., and SCHMITT R. A. (1989) Petrology of Apollo 14 regolith breccias and ion microprobe studies of glass beads. *Proc. Lunar Planet. Sci. Conf. 19th,* 1–17.

STANIN F. T. and TAYLOR L. A. (1980) Armalcolite: an oxygen fugacity indicator. *Proc. Lunar Planet. Sci. Conf. 11th,* 117–124.

UNRUH D. M., STILLE P., PATCHETT P. J., and TATSUMOTO M. (1984) Lu-Hf and Sm-Nd evolution in lunar mare basalts. *Proc. Lunar Planet Sci. Conf. 14th; J. Geophys. Res.* **89,** B459–B477.

USSELMAN T. M., LOFGREN G. E., DONALDSON C. H., and WILLIAMS R. J. (1975) Experimentally reproduced textures and mineral chemistries of high-titanium mare basalts. *Proc. Lunar Sci. Conf. 6th*, 997–1020.

VILLEMANT B., JAFFREZIC H., JORON J. L., and TREUIL M. (1981) Distribution coefficients of major and trace elements: fractional crystallization in the alkali basalt series of Chaine des Puys (Massif Central, France). *Geochim. Cosmochim. Acta* **45**, 1997–2016.

WARNER R. D., KEIL K., PRINZ M., LAUL J. C., MURALI A. V., and SCHMITT R. A. (1975) Mineralogy, petrology, and chemistry of mare basalts from Apollo 17 rake samples. *Proc. Lunar Sci. Conf. 6th*, 193–220.

WARNER R. D., KEIL K., and TAYLOR G. J. (1977) Coarse-grained basalt 71597: A product of partial olivine accumulation. *Proc. Lunar Sci. Conf. 8th*, 1429–1442.

WARNER R. D., TAYLOR G. J., CONRAD G. H., NORTHROP H. R., BARKER S., KEIL K., MA M.-S., and SCHMITT R. A. (1979) Apollo 17 high-Ti mare basalts: New bulk compositional data, magma types, and petrogenesis. *Proc. Lunar Planet. Sci. Conf. 10th*, 225–247.